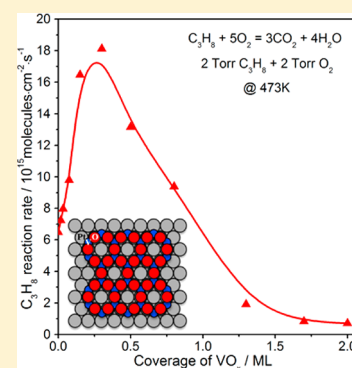


# Synergistic Effects of VO<sub>x</sub>–Pt Probed by the Oxidation of Propane on VO<sub>x</sub>/Pt(111)

Yanping Zheng, Lihua Zhang, Shaolin Wang, Ding Ding, Hong Zhang, Mingshu Chen,\* and Huilin Wan\*

State Key Laboratory of Physical Chemistry of Solid Surfaces, National Engineering Laboratory for Green Chemical Productions of Alcohols–Ethers–Esters, Department of Chemistry, College of Chemistry and Chemical Engineering, Xiamen University, Xiamen 361005, Fujian, China

**ABSTRACT:** VO<sub>x</sub>/Pt(111), which was grown layer-by-layer and exhibited a well-defined structure, was used as a model catalytic surface to study the intrinsic catalytic activity of Pt, as well as the effect of VO<sub>x</sub> additive, for the oxidation of propane. A special sample system was designed to ensure a reliable analysis of the trace amount of model catalytic reaction products. The results show that the catalytic activities for the oxidation of C<sub>3</sub>H<sub>8</sub> on the Pt(111) surface as adding VO<sub>x</sub> are suppressed apparently at temperatures below 400 K, but enhanced significantly at temperatures above 400 K. Maximum reaction rates are achieved at a VO<sub>x</sub> coverage of about 0.3 ML at the test temperatures of 423 and 473 K. The infrared reflection–absorption spectroscopy (IRAS) results show that the redox property of the VO<sub>x</sub>–Pt is much better than that of the bulklike VO<sub>x</sub>. This is confirmed by CO poisoning tests, in that the oxidation of VO<sub>x</sub>/Pt(111) is significantly suppressed by the coadsorbed CO. The kinetic data demonstrate that there are at least two catalytically active sites, metallic Pt and VO<sub>x</sub>–Pt interface, for the activation and oxidation of C<sub>3</sub>H<sub>8</sub>. The promotion effects of VO<sub>x</sub> on Pt for the oxidation of C<sub>3</sub>H<sub>8</sub> can be attributed to the synergism between VO<sub>x</sub> and Pt.



## 1. INTRODUCTION

Oxide-supported metal nanoparticles constitute a type of catalyst commonly used for catalytic application. The oxide used as a support not only changes the dispersion of the active metals but also modifies the activity and selectivity due to the interaction of the metal–oxide interface.<sup>1</sup> The oxide itself may also act as an active component synergistically enhancing the catalytic performance<sup>2–4</sup> or involving a bifunctional catalytic system.<sup>5</sup> Numerous researches demonstrated that the perimeter of metal–oxide boundaries plays a key role in the catalytic reactions, for examples, the oxidation of CO on Au/TiO<sub>2</sub>,<sup>6</sup> FeO/Pt(111),<sup>4</sup> MnO<sub>x</sub>-modified Ni(111)<sup>7</sup> and VO<sub>x</sub>/Rh(111),<sup>2</sup> water gas shift reaction on Au (or Pt)/CeO<sub>2</sub> and TiO<sub>x</sub> (or CeO<sub>x</sub>)/Au(111).<sup>3,8,9</sup>

Pt group metals have been extensively studied for the (selective) oxidation of hydrocarbons and used for the elimination of pollutants emitted by automotive exhaust and power plants.<sup>10–16</sup> Among which, platinum is the most active for the complete oxidation of propane at low temperature<sup>11</sup> and its activity is significantly affected by the nature of the supports and additives.<sup>12–15</sup> However, the effects of the supports and additives on the Pt-based catalysts for the oxidation of C<sub>3</sub>H<sub>8</sub>, as well as the intrinsic activity of Pt, remain unclear despite that a large number of researchers are focusing on this topic.<sup>12–15</sup> VO<sub>x</sub> is not only an effective additive for propane total oxidation<sup>14,15</sup> but also an active component for the partial oxidation of alkanes.<sup>17–30</sup> In this study, a single-crystal Pt(111) surface was used as a model catalyst to examine the effects of VO<sub>x</sub> additive on the activity for C<sub>3</sub>H<sub>8</sub> oxidation. Structural characterization and kinetic measurements demonstrated that the promoting effects of the VO<sub>x</sub> additive depend on the VO<sub>x</sub> coverage and reaction temperature. When combined with a home-built in situ infrared reflection

absorption spectrometer (IRAS),<sup>31</sup> the synergistic effect between Pt and VO<sub>x</sub> was found for the enhancements of VO<sub>x</sub> on Pt for the oxidation of C<sub>3</sub>H<sub>8</sub>.

## 2. EXPERIMENTAL SECTION

The experiments were performed in a combined elevated-pressure reaction cell–ultrahigh vacuum (UHV) system. Sample preparation and characterization were conducted in the primary UHV chamber (base pressure, 2 × 10<sup>−9</sup> Torr) equipped with an Auger electron spectrometer (AES) and a low-energy electron diffractometer (LEED). An elevated-pressure reaction cell is furnished with an IRAS for in situ collecting the surface information and an online Agilent gas chromatograph (GC) for evaluating the catalytic performance. ZnSe is used as in situ IRAS windows, and a home-built sample system (shown in Figure 1) is used for the kinetic studies. The two chambers are connected by a double-stage, differentially pumped Teflon sliding seal feedthrough,<sup>32</sup> which allows the sample to be transferred in situ into the elevated-pressure reaction cell. And the reaction cell can be performed at a pressure of UHV to 1000 Torr.

A new sampling system was designed to analyze the model catalytic reaction products using an online GC, as seen in Figure 1. With this new system, possible reaction products including CO, CO<sub>2</sub>, CH<sub>4</sub>, C<sub>2</sub>H<sub>4</sub>, C<sub>2</sub>H<sub>6</sub>, C<sub>3</sub>H<sub>6</sub>, and oxygenates for the oxidation of C<sub>3</sub>H<sub>8</sub> in the reaction cell with a pressure of just several Torr (much lower than the atmosphere pressure of 760 Torr) can be efficiently compressed into the GC sample loop and injected into the GC columns for quantitative analyses with high sensitivity. Typically, approximately 80% of the mixture of the reactants and reaction products in the reaction cell can be injected into the GC sample loop, leading to a possible detection limit of

Received: April 4, 2013

Revised: June 13, 2013

Published: June 13, 2013

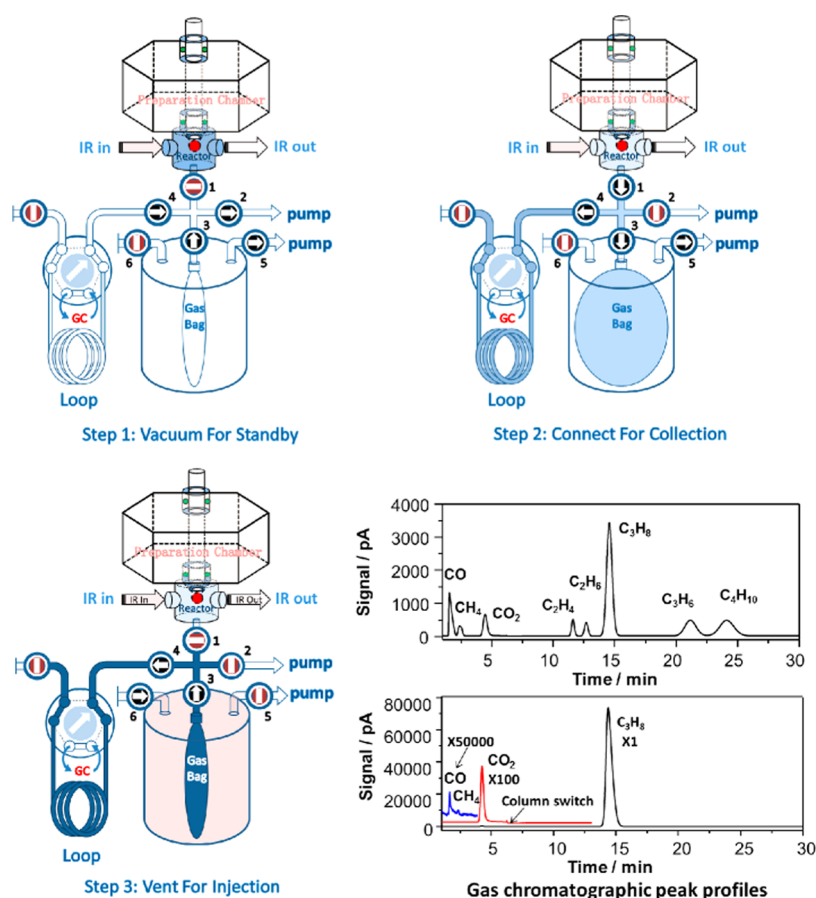


**Figure 1.** Schematic diagram of the sample system for compressing the model reaction mixtures from the in situ reaction cell into the online GC sample loop for quantitative analyses. Step 1, the gas bag that was mounted in a vacuum chamber is pumped to vacuum; step 2, the reaction mixtures are inflated into the gas bag; step 3, the reaction mixture in the gas bag is compressed into the GC sample loop and being ready to be injected into the GC columns. A typical GC peak profile for a gas mixture of  $\text{O}_2$ ,  $\text{CO}$ ,  $\text{CH}_4$ ,  $\text{CO}_2$ ,  $\text{C}_2\text{H}_4$ ,  $\text{C}_2\text{H}_6$ ,  $\text{C}_3\text{H}_8$ ,  $\text{C}_3\text{H}_6$ , and iso- $\text{C}_4\text{H}_{10}$ , and a peak profile for reaction products of the oxidation of  $\text{C}_3\text{H}_8$  on Pt, are displayed.

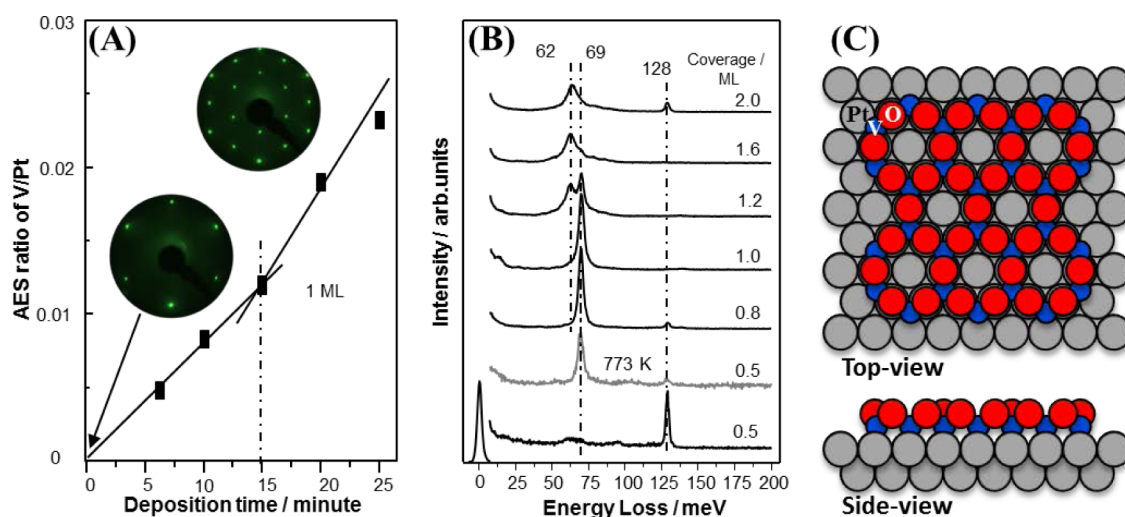


**Figure 2.** (A) V/Pt AES ratios as a function of the deposition time. (B) High-resolution electron energy loss (HREEL) spectra of  $\text{VO}_x$  on Pt(111) with various coverages. (C) Top and side views of a possible structure model for the  $\text{V}_2\text{O}_3/\text{Pt}(111)$  overlayer with a  $(2 \times 2)$  arrangement. The films were grown at 623 K.

$10^{-12}$  mol. Note that the detection limit for an Agilent FID detector is claimed to be 1.8 pgC/s. A regular GC sampling for most model catalysis studies can only inject a very small amount of reaction mixture into the GC column that is not sensitive enough, and the liquid nitrogen trap can only collect those components with high boiling points.<sup>33</sup> For the

oxidation of  $\text{C}_3\text{H}_8$ , some of the possible reaction products, like  $\text{CO}$ ,  $\text{CH}_4$ , etc., cannot be trapped at the liquid nitrogen temperature under vacuum conditions.

The Pt(111) single crystal (diameter of 10 mm, thickness of 1 mm) was mounted by a tantalum wire. The sample is resistively heated. A W–

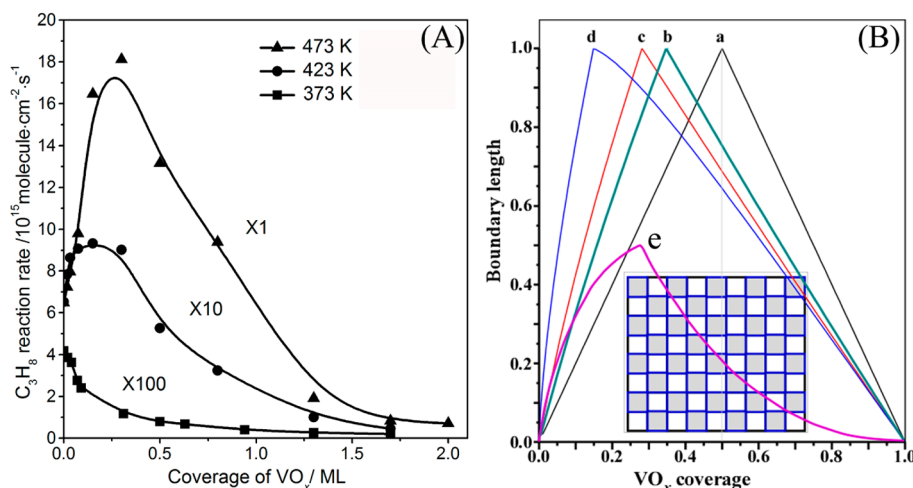


**Figure 3.** (A) Reaction rates for the oxidation of  $C_3H_8$  on the  $VO_x/Pt(111)$  surfaces as a function of the  $VO_x$  coverage at 373, 423, and 473 K, respectively.  $C_3H_8/O_2 = 1:1$ ,  $P_{total} = 4$  Torr. The total reaction times were adjusted to be 60, 10, and 2.5 min for the reaction temperatures of 373, 423, and 473 K, respectively. (B) Simple statistic plots of the lengths of the perimeters of  $V_2O_3$  2D domains as a function of the  $V_2O_3$  coverage ( $\theta$ ): (a) ideal case; (b–d) the factors of domain size increase were assumed to be 0.5%, 1% and 10%; (e) the factor of domain size increase was assumed to be 1% and the probability of merging domains together was set to be 1%. The details of such simulation are shown in ref 39.

5%Re/W–26%Re thermocouple was spot-welded on the sample edge for the temperature measurements. The Pt(111) surfaces (both sides) were cleaned through repeated cycles of  $Ar^+$  sputtering (2 keV, 5  $\mu A$ ) at 300 K, followed by oxidation ( $P_{O_2} = 5 \times 10^{-7}$  Torr) at 700 K, and finally by annealing at 1100 K. The cleanness of the surface was confirmed by AES and a sharp ( $1 \times 1$ ) LEED pattern. The  $VO_x/Pt(111)$  model surfaces were prepared via deposition of metallic vanadium from a filament source onto the Pt(111) surfaces (both sides) at room temperature, followed by an oxidation at 623 K for 10 min and cooling to room temperature in  $1 \times 10^{-7}$  Torr  $O_2$ . The  $VO_x$  coverage was calibrated using the V/Pt AES ratio.

After the preparation and characterization in the UHV chamber, the sample was transferred in situ into the elevated-pressure reaction cell (0.5 L). Ultrahigh-purity  $O_2$  (Hong Kong Specialty Gases Co., Ltd.) and research-purity (99.999%) propane (Foshan Kodi Gas Chemical Industry Co., Ltd.) were further purified using a constant temperature trap at the melting point of ethyl acetate before used. Typically, a  $C_3H_8/O_2$  (1:1) mixture with a total pressure of 4 Torr was introduced into the reaction cell at room temperature and then rapidly heated to the desired temperature to initiate the kinetic measurements. After specific reaction duration, the reaction gas mixture was pumped into the home-built sample system and compressed into the GC sample loop for product analyzing, as shown in Figure 1. The product analysis was performed using a gas chromatograph (Agilent 7890) equipped with an  $Al_2O_3$ -squalane column and a Porapak Q packed column, a thermal conductivity detector (TCD), a flame ionization detector (FID), and a methanation converter. The rate of propane conversion is expressed as molecules· $cm^{-2}$ · $s^{-1}$ , which is calculated as molecules of  $C_3H_8$  converted per square centimeter surface area per second.

### 3. RESULTS AND DISCUSSION

**3.1. Growth and Characterization of  $VO_x/Pt(111)$  Model Surfaces.**  $VO_x/Pt(111)$  was grown layer-by-layer on the Pt(111) surface by deposition of V in  $1 \times 10^{-7}$  Torr  $O_2$  at 623 K, as evidenced by the linear increase of the V/Pt AES ratios as a function of the deposition time and a distinct breakpoint (Figure 2A). Figure 2B shows high-resolution electron energy loss (HREEL) spectra of various  $VO_x$  structures on Pt(111). The  $VO_x/Pt(111)$  at the coverage below 0.5 ML shows a strong phonon at 128 meV (1032  $cm^{-1}$ ), which can be attributed to the  $V=O$  stretching mode of  $O=VO_x$  species.<sup>34,35</sup> It is worth noting that such an  $O=VO_x$  species is unstable and forms two-dimensional (2D) surface  $V_2O_3$  domains on the Pt(111) surface

upon annealing in UHV (the second line from the bottom in Figure 2B) or coadsorption with CO at room temperature, as evidenced by a strong phonon appearing at 69 meV (556  $cm^{-1}$ ), which has been assigned to the asymmetric vibration of  $V^{3+}-O-V^{3+}$ .<sup>36,37</sup> When the coverage is further increased up to 1 ML, the phonon peak at 128 meV disappears and the 69 meV phonon appears, which exhibits a sharp ( $2 \times 2$ ) LEED pattern (see the insets in Figure 2A). Such results reveal the formation of 2D  $V_2O_3$  domains at submonolayer and an overlayer at 1 ML. On the basis of these experimental results and the structural models proposed for the  $V_2O_3/Rh(111)$  and  $V_2O_3/Pd(111)$ ,<sup>38</sup> a similar structure model was proposed as shown in Figure 2C. At above 1 ML, a new phonon at 62 meV (500  $cm^{-1}$ ) appears and completely replaces the 69 meV phonon at 2 ML. This can be assigned to the formation of a bilayer  $z'-VO_x$ .<sup>38</sup>

**3.2. Kinetics Study of the Oxidation of Propane.** The reaction kinetics of  $C_3H_8$  oxidation was performed on the Pt(111) and  $VO_x/Pt(111)$  surfaces with various  $VO_x$  coverages at 373, 423, and 473 K, respectively. In the present reaction conditions, the main products were  $CO_2$  and  $H_2O$ . Selective oxidation products, like propylene, oxygenates, and CO, were either not detected or below 0.1% of the combustion product  $CO_2$ . This is consistent with previous reports that propane is mainly completely oxidized on the supported and bulklike Pt catalysts.<sup>11–14</sup> Figure 3A shows the specific reaction rate for the oxidation of  $C_3H_8$  as a function of the  $VO_x$  coverage. Clean Pt surface is active for the oxidation of  $C_3H_8$ . At 373 K, the reaction rate for the oxidation of  $C_3H_8$  on the  $VO_x/Pt(111)$  decreases as the  $VO_x$  coverage increases. In contrast, when the reaction temperature reaches 423 K, the reaction rate increases significantly with the increase of the  $VO_x$  coverage until a maximum is reached at a  $VO_x$  coverage of about 0.3 ML, then decreases with further increasing the  $VO_x$  coverage. At 473 K, such enhancements of the reaction rates for  $C_3H_8$  oxidation on  $VO_x/Pt(111)$  are more significant.

**3.3. IRAS Study of the Redox Properties.** The redox properties of a catalyst are crucial for oxidation reactions because most hydrocarbon oxidation reactions occur via the Mars–van Krevelen mechanism, which involves redox cycles of the catalytic active components during the reactions.<sup>29,40</sup> Two typical

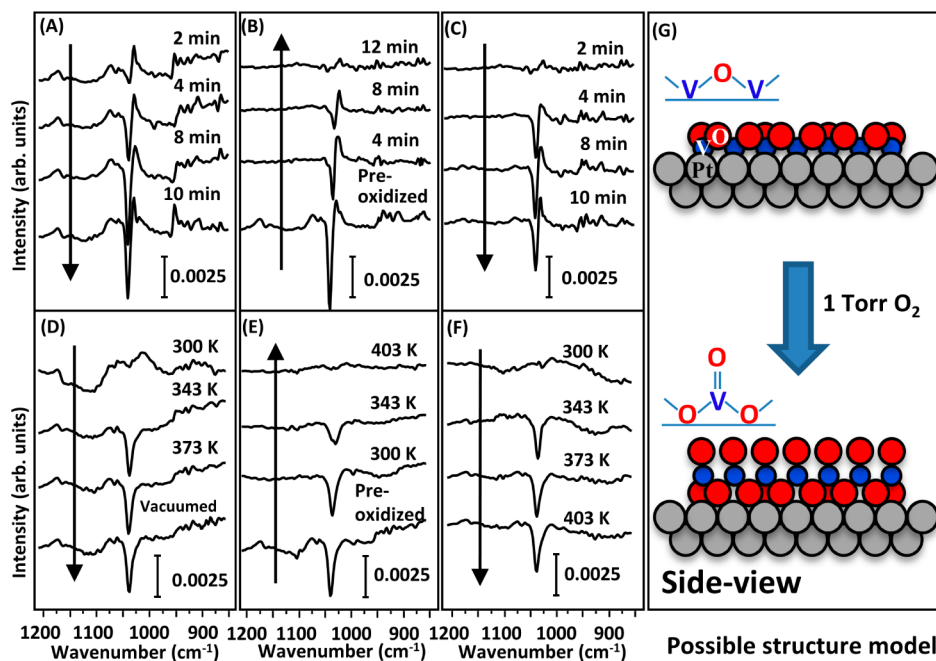


**Figure 4.** IRAS spectra for the 0.9 ML  $\text{VO}_x/\text{Pt}(111)$  exposed to (A) 1 Torr  $\text{O}_2$ , (B) 1 Torr  $\text{C}_3\text{H}_8$ , and (C) a mixture of 1 Torr  $\text{O}_2$  and 1 Torr  $\text{C}_3\text{H}_8$ , at 300 K and for the 3 ML  $\text{VO}_x/\text{Pt}(111)$  exposed to (D) 1 Torr  $\text{O}_2$ , (E) 1 Torr  $\text{C}_3\text{H}_8$ , (F) a mixture of 1 Torr  $\text{O}_2$  and 1 Torr  $\text{C}_3\text{H}_8$ ; (G) side view of a possible structure model for the  $\text{V}_2\text{O}_3/\text{Pt}(111)$  under vacuum (up) and exposed to 1 Torr  $\text{O}_2$  (down).

surfaces, partially (0.9 ML  $\text{VO}_x$ ) and completely (3 ML  $\text{VO}_x$ ) covered Pt(111) surfaces, corresponding to  $\text{VO}_x$ -Pt interface and  $\text{VO}_x$  surfaces, respectively, were chosen to compare the redox properties of Pt(111)-supported  $\text{VO}_x$  by exposing the samples prepared under UHV condition to 1 Torr of oxygen and  $\text{C}_3\text{H}_8$ , respectively, and tracked by the home-built in situ IRAS.<sup>31</sup> The results are compared in Figure 4. When the 0.9 ML  $\text{VO}_x/\text{Pt}(111)$  was exposed to 1 Torr  $\text{O}_2$  at room temperature, a vibration peak at  $1038\text{ cm}^{-1}$  corresponding to the  $\text{V}=\text{O}$  vibration appeared, as seen in Figure 4A. This peak intensity increased with the exposure time and reached stable at an exposure time of 10 min. Note that, before exposing to 1 Torr  $\text{O}_2$ , the  $\text{VO}_x$  film was a surface  $\text{V}_2\text{O}_3$ . The appearance of  $\text{V}=\text{O}$  indicates the oxidation of the  $\text{V}_2\text{O}_3/\text{Pt}(111)$ , as shown by a proposed model in Figure 4G. The so-formed  $\text{V}=\text{O}$  species was stable under the UHV conditions, but reduced as exposed to  $\text{C}_3\text{H}_8$  at room temperature (Figure 4B) and reoxidized after exposing to a mixture of 1 Torr  $\text{O}_2$  and 1 Torr  $\text{C}_3\text{H}_8$  (Figure 4C). These results reveal that the  $\text{VO}_x$ -Pt interface exhibits high redox properties at room temperature.

In comparison, for exposing the 3 ML  $\text{VO}_x/\text{Pt}(111)$  to 1 Torr  $\text{O}_2$ , the IR intensity of  $\text{V}=\text{O}$  species did not increase at room temperature, but at 343–373 K (Figure 4D). The so-formed  $\text{V}=\text{O}$  bonds were hardly reduced by  $\text{C}_3\text{H}_8$  at room temperature, but completely reduced at 403 K, as seen in Figure 4E. The reduced surface required a higher temperature to recover the  $\text{V}=\text{O}$  species upon exposing to the mixture of 1 Torr  $\text{C}_3\text{H}_8$  and 1 Torr  $\text{O}_2$ . These results reveal that the redox properties of the submonolayer  $\text{VO}_x/\text{Pt}(111)$  is much better than that of the multilayer one, i.e., the  $\text{VO}_x$ -Pt interface is better than the bulklike  $\text{VO}_x$ . Such difference should be related to the substrate Pt surface, either by an electronic modification or directly involving the activation of  $\text{O}_2$  and  $\text{C}_3\text{H}_8$ . CO poisoning tests were performed to distinguish these two effects, as shown in Figure 5. When the preoxidized submonolayer  $\text{O}=\text{VO}_x/\text{Pt}(111)$  surface is exposed to 1 Torr CO, there appears a vibration peak at  $2085$

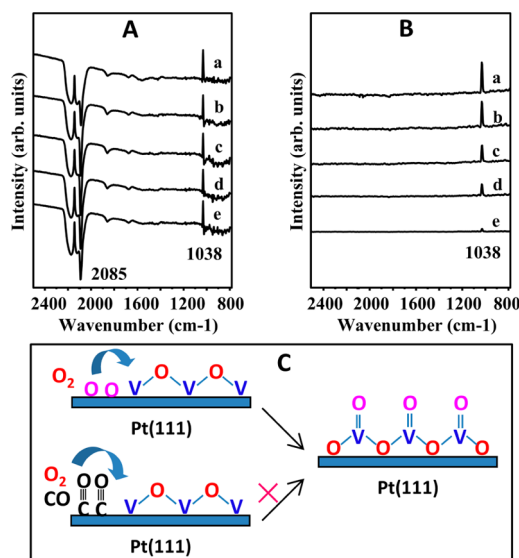


**Figure 5.** IRAS spectra for the preoxidized 0.9 ML  $\text{VO}_x/\text{Pt}(111)$  surface at room temperature (A) exposed to 1 Torr CO (a), a mixture of 1 Torr  $\text{O}_2$  and 1 Torr CO for 2, 4, 8, and 10 min, respectively (b–e); (B) reduced by  $\text{C}_3\text{H}_8$  (a), exposed to 1 Torr  $\text{O}_2$  for 2, 4, 8, and 10 min, respectively (b–e). The preoxidized 0.9 ML  $\text{VO}_x/\text{Pt}(111)$  surface was used as the background spectrum. (C) Schematic formation paths of  $\text{O}=\text{VO}_x$  on Pt(111) from  $\text{V}_2\text{O}_3$  without (upper) and with (lower) presence of CO.

$\text{cm}^{-1}$  corresponding to the atop adsorbed CO on the Pt surface<sup>41</sup> and a reversed peak at  $1038\text{ cm}^{-1}$  indicating the reduction of  $\text{V}=\text{O}$  by CO (Figure 5A). Then when such reduced and CO-adsorbed  $\text{VO}_x/\text{Pt}(111)$  surface is exposed to a mixture of 1 Torr  $\text{O}_2$  and 1 Torr CO at room temperature, the reversed peak of  $\text{V}=\text{O}$  failed to be resumed, i.e., the reduced  $\text{VO}_x/\text{Pt}(111)$  cannot be oxidized to  $\text{O}=\text{VO}_x/\text{Pt}(111)$  in the presence of CO. In contrast, such reversed  $\text{V}=\text{O}$  peak resumed eventually by

exposure to O<sub>2</sub> only without CO (Figure 5B). These experiments evidenced that the redox properties of VO<sub>x</sub> were promoted by uncovered Pt, probably due to the spillover of oxygen from Pt sites to VO<sub>x</sub> (Figure 5C), regarding that O<sub>2</sub> can be dissociated adsorbed on Pt surfaces below room temperature.<sup>42,43</sup>

**3.4. Synergistic Effects.** Kinetic results show that Pt only is active for the oxidation of C<sub>3</sub>H<sub>8</sub> even at low temperature ( $\theta_{\text{VO}_x} = 0$ , Figure 3A). A turnover frequency (TOF) of about 0.001 C<sub>3</sub>H<sub>8</sub> molecules converted per second per surface Pt atom was obtained at 313 K as shown in Figure 6. The monotonic decrease

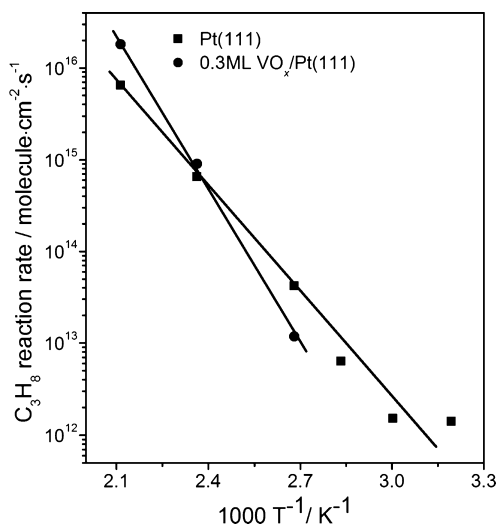


**Figure 6.** Arrhenius plots of the C<sub>3</sub>H<sub>8</sub> conversion rate on the clean Pt(111) and 0.3 ML VO<sub>x</sub>/Pt(111) surfaces.

of the reaction rate obtained at 373 K as adding VO<sub>x</sub> onto the Pt(111) surface (Figure 3A) demonstrates that the VO<sub>x</sub> sites are less active than the surface Pt sites. Moreover, the VO<sub>x</sub> blocks the surface-active Pt sites. This is consistent with the high adsorption/activation barrier of C<sub>3</sub>H<sub>8</sub> (80–130 kJ/mol) on vanadia-based catalysts.<sup>44</sup> A higher reaction temperature (450–700 K) is generally required for the oxidation of C<sub>3</sub>H<sub>8</sub> on vanadia-based catalysts.<sup>44</sup> In fact, the reaction rate for the oxidation of C<sub>3</sub>H<sub>8</sub> on a VO<sub>x</sub>/Pt(111) surface is significantly lower than that on the clean Pt surface, especially when the Pt surface is completely covered by VO<sub>x</sub> ( $\theta_{\text{VO}_x} > 1$  ML, Figure 3A). These results support that the promotion effects of Pt on the redox properties of VO<sub>x</sub> may benefit from the spillover of oxygen from Pt sites to VO<sub>x</sub>.

In contrast, at 423 and 473 K, the reaction rate for the oxidation of C<sub>3</sub>H<sub>8</sub> increased significantly as adding a small amount of VO<sub>x</sub> onto the Pt(111) surface. Maximum reaction rates are achieved at a VO<sub>x</sub> coverage of about 0.3 ML (Figure 3A). Statistic plots of the lengths of 2D VO<sub>x</sub> domain boundary as a function of the coverage are shown in Figure 3B.<sup>41</sup> Since the VO<sub>x</sub> overlayer forms small 2D domains on the Pt(111) surface, the domain sizes and the total Pt surface area covered by VO<sub>x</sub> increase with the VO<sub>x</sub> coverage. However, the maximum length of the domain boundary of VO<sub>x</sub> occurs at a low VO<sub>x</sub> coverage which depends on the average size and size distribution of the domains, as shown in Figure 3B. The similarity of the curve shapes between the reaction rate of C<sub>3</sub>H<sub>8</sub> oxidation and the statistic length of the domain boundary as a function of the VO<sub>x</sub> coverage on Pt(111) proposed that the interface of the VO<sub>x</sub>–Pt is the most active region at above 400 K. This suggests that the most active sites should be the boundary of the 2D VO<sub>x</sub> domains

on the Pt(111) surface. This is in line with that the redox properties of VO<sub>x</sub> for the submonolayer VO<sub>x</sub>/Pt(111) is much better than that of the multilayer VO<sub>x</sub>/Pt(111) from IRAS study (Figure 4). The significance of the interface domain boundary has been well-established in literature, for examples, CO oxidation on Au/TiO<sub>2</sub>,<sup>6</sup> FeO/Pt(111),<sup>4</sup> MnO<sub>x</sub>-modified Ni(111),<sup>7</sup> and VO<sub>x</sub>/Rh(111),<sup>2</sup> water gas shift reaction on CeO<sub>x</sub> (or TiO<sub>2</sub>)/Au(111),<sup>3</sup> and 1-butene hydroisomerization on Pt/Grafoil.<sup>45</sup> Where the best catalytic reaction rates, as well as the length of the boundary, were also reported to be at a surface coverage of around 30% of the total substrate area.<sup>3,4</sup>

The above results and discussion show that Pt can promote the redox properties of VO<sub>x</sub> and VO<sub>x</sub> can promote the catalytic activity for the oxidation of propene on Pt. The former may be due to the spillover of oxygen from the surface Pt sites to VO<sub>x</sub>. The latter can be understood from the following discussions. First, although Pt is active for C<sub>3</sub>H<sub>8</sub> oxidation at low temperatures (see Figures 3A and 6), it was reported that the initial sticking probability of C<sub>3</sub>H<sub>8</sub> molecules on the Pt surface is very low,<sup>16,46,47</sup> particularly in the presence of oxygen in which C<sub>3</sub>H<sub>8</sub> adsorption is energetically competitive with oxygen.<sup>48</sup> This can be realized from that the reaction rate of CO oxidation is 2–3 orders of magnitude higher than that of C<sub>3</sub>H<sub>8</sub> oxidation on Pt at a similar reaction temperature, i.e., the activation of O<sub>2</sub> is much faster than that of C<sub>3</sub>H<sub>8</sub>, leading to a chemisorbed oxygen dominant surface.<sup>31,49</sup> Such oxygen-dominant Pt surface may suppress the activation/dissociation of C<sub>3</sub>H<sub>8</sub>, leading to a low reaction rate of the oxidation of C<sub>3</sub>H<sub>8</sub>, as evidenced by a negative reaction order to oxygen for the oxidation of C<sub>3</sub>H<sub>8</sub> on Pt catalysts.<sup>13,50</sup> Second, many studies showed that the reaction rates for the oxidation of C<sub>3</sub>H<sub>8</sub> on Pt-based catalysts were promoted significantly by additives which also enhanced the sticking probability of C<sub>3</sub>H<sub>8</sub>.<sup>13,16</sup> Wilson et al.<sup>16</sup> reported that the initial sticking probability at 300 K for the chemisorption of C<sub>3</sub>H<sub>8</sub> on the clean Pt surface increased from an immeasurable value to 0.02 ± 0.01 on the SO<sub>2</sub> promotion surface, resulting in a significant enhancement of the dissociative chemisorption and subsequent combustion of C<sub>3</sub>H<sub>8</sub>. Zeolite was also found to enhance the uptake of C<sub>3</sub>H<sub>8</sub>, leading to more than 2 orders of magnitude enhancement in the propane combustion rate.<sup>13</sup> It is general that acid can strengthen the adsorption of alkane molecules.<sup>51,52</sup> The enhancement of activity for the oxidation of C<sub>3</sub>H<sub>8</sub> on Pt catalysts promoted by an acid VO<sub>x</sub> additive<sup>15</sup> may be considered as increasing the initial sticking probability of C<sub>3</sub>H<sub>8</sub>. In fact, deduced from the Arrhenius plots in Figure 6, the pre-exponential factor is 1.7 × 10<sup>28</sup> molecules·cm<sup>-2</sup>·s<sup>-1</sup> for C<sub>3</sub>H<sub>8</sub> oxidation on the 0.3 ML VO<sub>x</sub>/Pt(111), which is more than 4 orders of magnitude higher than that of 9.1 × 10<sup>23</sup> molecules·cm<sup>-2</sup>·s<sup>-1</sup> on the Pt(111).

Figure 6 shows Arrhenius plots of the C<sub>3</sub>H<sub>8</sub> oxidation on the clean Pt(111) and 0.3 ML VO<sub>x</sub>/Pt(111) surfaces. The apparent activation energies are 74 and 108 kJ/mol for the Pt(111) and 0.3 ML VO<sub>x</sub>/Pt(111) surfaces, respectively. Note that it is difficult to estimate the activation energy for the oxidation of C<sub>3</sub>H<sub>8</sub> on the multilayer VO<sub>x</sub>/Pt due to the significantly low reaction rates under the present examined conditions. The plots for 0.3 ML VO<sub>x</sub> and Pt(111) intersect at 400 K (threshold temperature). These results suggest that, below 400 K, the reaction rate for the oxidation of C<sub>3</sub>H<sub>8</sub> on the VO<sub>x</sub>–Pt interface is lower than that on the platinum surface even though C<sub>3</sub>H<sub>8</sub> can be oxidized on the VO<sub>x</sub>/Pt(111) surface at room temperature (as shown by the IRAS data in Figure 4 that VO<sub>x</sub> can be oxidized by oxygen and subsequently reduced by C<sub>3</sub>H<sub>8</sub>). Thus, below the threshold

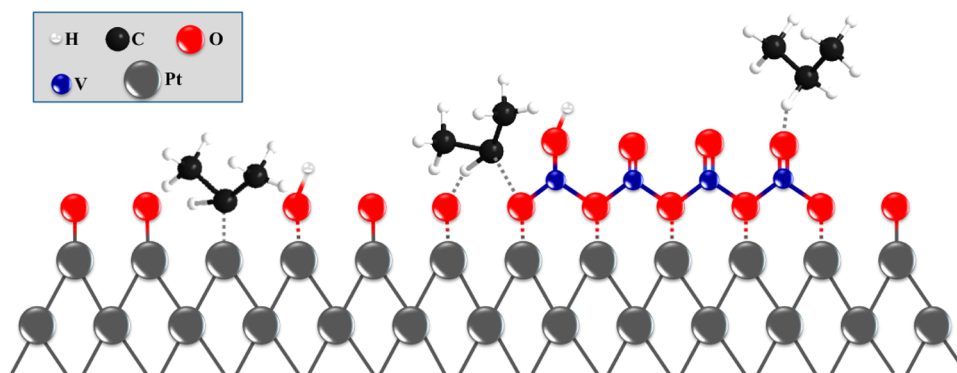


**Figure 7.** Simple schematics of the proposed activation paths for  $C_3H_8$  on the Pt(111) and  $VO_x/Pt(111)$  surfaces.

temperature, the less active  $VO_x$  species locates on the much active Pt sites, leading to a decrease of the total activity. Above this temperature, due to that  $C_3H_8$  oxidation on the  $VO_x$ -Pt interface is now faster than that on the Pt-only sites, the total reaction rate increased as the  $VO_x$  coverage increased. A maximum reaction rate was achieved at about 0.3 ML, and above 1 ML (corresponding to a complete cover of the Pt surface by  $VO_x$ ) the rate was significantly lower than that on the clean Pt surface. This result is consistent with the IRAS results, which show that the redox properties and the reactivity to  $C_3H_8$  of the multilayer  $VO_x$  are lower than those on the submonolayer  $VO_x$ , i.e.,  $VO_x$ -Pt interface.

The apparently different effects at below and above 400 K suggest that there exist at least two kinds of surface-active sites, the surface Pt sites and  $VO_x$ -Pt interface sites, and that the electronic effect may not be the key role corresponding to the promotion effects of  $VO_x$  on Pt for the oxidation of  $C_3H_8$ . Synergistic effects between the  $VO_x$  and Pt may correspond to the promotion by  $VO_x$ . Figure 7 shows the simple schematics of the activation of  $C_3H_8$  at the O/Pt surface and  $VO_x$ -Pt(111) interface. On the Pt surface,  $C_3H_8$  is activated at the Pt sites associated with the surface chemisorbed oxygen, but it is somewhat suppressed if the coverage of the surface oxygen is near saturate. On the  $VO_x$ -Pt interface,  $C_3H_8$  is activated either at the  $O=VO_x$  group or at the Pt sites neighboring to the  $VO_x$  and may be associated with chemisorbed oxygen on the Pt surface. And the Pt surface may supply active oxygen for reoxidizing the  $VO_x$  species during the catalytic reaction, resulting in a significant enhancement of the catalytic activity.

Supported vanadia has been extensively studied for the oxidative dehydrogenation of propane (ODP) in the past 3 decades.<sup>17–22</sup> Especially, the isolated  $VO_x$  species has been shown to possess a much higher selectivity for  $C_3H_6$ .<sup>23,24,53</sup> The lower coverage  $VO_x/Pt$  was hence expected to produce some selective oxidation products, like  $C_3H_6$  and CO. However, the unselective product of  $CO_2$  was found as the main product in the present study. This may be due to the presence of Pt and sufficient  $O_2$ . Note that, although a typical  $C_3H_8/O_2$  ratio of 1:1 was used, the conversion rate was normally controlled to be below 10%, i.e., only a small amount of  $O_2$  was consumed. Numerous studies have shown that  $CO_2$  was the main product for the oxidation of  $C_3H_8$  on Pt-based catalysts.<sup>11–16</sup> Except in some special cases, like subnanoscale Pt particles ( $Pt_{8–10}$ ),<sup>54</sup> very short contact time,<sup>55</sup> and high reaction temperature,<sup>56</sup> partial oxidation products were observed. In fact, even on a supported vanadia catalyst, it may turn to be unselective if the  $O_2/C_3H_8$  ratio is high.<sup>57–59</sup> And it was reported that the  $AlVO_x$  species calcined at 753 K is selective for ODP but becomes less active,

and totally unselective (produced only  $CO_2$ ), after being calcined at 973 K.<sup>60</sup> Obviously, the activity and selectivity of a vanadia catalyst are not only related to the structure of  $VO_x$  but also the bond strength of the oxygen, reaction atmosphere, and other aspects. More work is required to understand the mechanisms for the oxidation of alkanes.

#### 4. CONCLUSIONS

A special sample system was successfully designed for model catalysis studies, which can guarantee a reliable analysis of the trace amount of reaction products, especially for the catalytic conversion of light alkanes in the presence of oxygen. Two catalytic active sites exist on the  $VO_x/Pt(111)$  surface for  $C_3H_8$  oxidation: Pt-only sites present a lower activation energy but a low sticking probability on an oxygen-rich surface; the interface of the  $VO_x$ -Pt possesses a higher activation energy but higher sticking probability. Such characteristic results in that  $C_3H_8$  is predominantly oxidized on the Pt sites at low temperatures, while on the  $VO_x$ -Pt interface at higher temperature. The number of the active  $VO_x$ -Pt interface sites (boundary of the  $VO_x$  domains) is a function of the  $VO_x$  coverage on Pt(111), leading to a maximum reaction rate observed at a  $VO_x$  coverage of about 0.3 ML. The high reaction rate that occurred at the  $VO_x$ -Pt interface can be contributed to the synergistic effects, in that Pt promotes the redox properties of  $VO_x$  and the  $VO_x$  enhances the sticking probability of  $C_3H_8$ . These results should help in designing more efficient catalysts for oxidation and partial oxidation reactions.

#### ■ AUTHOR INFORMATION

##### Corresponding Author

\*Phone: 86-592-2183723 (M.C.); 86-592-2186569 (H.W.). Fax: 86-592-2183723 (M.C.); 86-592-2185192 (H.W.). E-mail: chenms@xmu.edu.cn (M.C.); hlwan@xmu.edu.cn (H.W.).

##### Notes

The authors declare no competing financial interest.

#### ■ ACKNOWLEDGMENTS

We gratefully acknowledge the support of this work by the National Basic Research Program of China (973 program: 2010CB732303, 2013CB933102), the Major Project of the Chinese Ministry of Education (no. 309019), the National Natural Science Foundation of China (20923004, 21033006, 21073149, 21273178), the Program for Changjiang Scholars and Innovative Research Team in University (no. IRT1036), and the Ph.D. Programs Foundation of the Chinese Ministry of Education (no. 20110121110010).

## REFERENCES

- (1) Ertl, G.; Knözinger, H.; Schüth, F.; Weitkamp, J. *Handbook of Heterogeneous Catalysis*; John Wiley and Sons: Weinheim, Germany, 1999.
- (2) Krenn, G.; Schoiswohl, J.; Surnev, S.; Netzer, F. P.; Schennach, R. Metal-oxide boundary effects in vanadium oxide–Rh(111) inverse model catalysts: a RAIRS, STM and TPD study. *Top. Catal.* **2007**, *46*, 231–238.
- (3) Rodriguez, J. A.; Ma, S.; Liu, P.; Hrbek, J.; Evans, J.; Pérez, M. Activity of CeO<sub>x</sub> and TiO<sub>x</sub> nanoparticles grown on Au(111) in the water-gas shift reaction. *Science* **2007**, *318*, 1757–1760.
- (4) Fu, Q.; Li, W. X.; Yao, Y.; Liu, H. Y.; Su, H. Y.; Ma, D.; Gu, X. K.; Chen, L. M.; Wang, Z.; Zhang, H.; Wang, B.; Bao, X. H. Interface-confined ferrous centers for catalytic oxidation. *Science* **2010**, *328*, 1141–1144.
- (5) Kang, J.; Cheng, K.; Zhang, L.; Zhang, Q.; Ding, J.; Hua, W.; Lou, Y.; Zhai, Q.; Wang, Y. Mesoporous zeolite-supported ruthenium nanoparticles as highly selective Fischer–Tropsch catalysts for the production of C<sub>5</sub>–C<sub>11</sub> isoparaffins. *Angew. Chem.* **2011**, *123*, 5306–5309.
- (6) Chen, M. S.; Goodman, D. W. Catalytically active gold on ordered titania supports. *Chem. Soc. Rev.* **2008**, *37*, 1860–1870.
- (7) Zhao, Y. B.; Chung, Y. W. CO chemisorption over MnO<sub>x</sub>-modified Ni(111): Importance of perimeter sites in strong metal-support interaction. *J. Catal.* **1987**, *106*, 369–377.
- (8) Fu, Q.; Saltsburg, H.; Flytzani-Stephanopoulos, M. Active nonmetallic Au and Pt species on ceria-based water-gas shift catalysts. *Science* **2003**, *301*, 935–938.
- (9) Vayssilov, G. N.; Lykhach, Y.; Migani, A.; Staudt, T.; Petrova, G. P.; Tsud, N.; Skála, T.; Bruix, A.; Illas, F.; Prince, K. C.; Matolín, V. r.; Neyman, K. M.; Libuda, J. Support nanostructure boosts oxygen transfer to catalytically active platinum nanoparticles. *Nat. Mater.* **2011**, *10*, 310–315.
- (10) Taylor, M. N.; Zhou, W.; Garcia, T.; Solsona, B.; Carley, A. F.; Kiely, C. J.; Taylor, S. H. Synergy between tungsten and palladium supported on titania for the catalytic total oxidation of propane. *J. Catal.* **2012**, *285*, 103–114.
- (11) Choudhary, T. V.; Banerjee, S.; Choudhary, V. R. Catalysts for combustion of methane and lower alkanes. *Appl. Catal., A* **2002**, *234*, 1–23.
- (12) Burch, R.; Halpin, E.; Hayes, M.; Ruth, K.; Sullivan, J. A. The nature of activity enhancement for propane oxidation over supported Pt catalysts exposed to sulphur dioxide. *Appl. Catal., B* **1998**, *19*, 199–207.
- (13) Garetto, T. F.; Rincón, E.; Apesteguía, C. R. Deep oxidation of propane on Pt-supported catalysts: drastic turnover rate enhancement using zeolite supports. *Appl. Catal., B* **2004**, *48*, 167–174.
- (14) Yoshida, H.; Yazawa, Y.; Hattori, T. Effects of support and additive on oxidation state and activity of Pt catalyst in propane combustion. *Catal. Today* **2003**, *87*, 19–28.
- (15) Avila, M. S.; Vignatti, C. I.; Apesteguía, C. R.; Rao, V. V.; Chary, K.; Garetto, T. F. Effect of V<sub>2</sub>O<sub>5</sub> loading on propane combustion over Pt/V<sub>2</sub>O<sub>5</sub>–Al<sub>2</sub>O<sub>3</sub> catalysts. *Catal. Lett.* **2010**, *134*, 118–123.
- (16) Wilson, K.; Hardacre, C.; Lambert, R. M. SO<sub>2</sub>-promoted chemisorption and oxidation of propane over Pt (111). *J. Phys. Chem.* **1995**, *99*, 13755–13758.
- (17) Gao, X. T.; Ruiz, P.; Xin, Q.; Guo, X. X.; Delmon, B. Effect of coexistence of magnesium vanadate phases in the selective oxidation of propane to propene. *J. Catal.* **1994**, *148*, 56–67.
- (18) Mamedov, E. A.; Cortés Corberán, V. Oxidative dehydrogenation of lower alkanes on vanadium oxide-based catalysts. The present state of the art and outlooks. *Appl. Catal., A* **1995**, *127*, 1–40.
- (19) Blasco, T.; Nieto, J. M. L. Oxidative dehydrogenation of short chain alkanes on supported vanadium oxide catalysts. *Appl. Catal., A* **1997**, *157*, 117–142.
- (20) Khodakov, A.; Olthof, B.; Bell, A. T.; Iglesia, E. Structure and catalytic properties of supported vanadium oxides: Support effects on oxidative dehydrogenation reactions. *J. Catal.* **1999**, *181*, 205–216.
- (21) Liu, Y. M.; Cao, Y.; Yi, N.; Feng, W. L.; Dai, W. L.; Yan, S. R.; He, H. Y.; Fan, K. N. Vanadium oxide supported on mesoporous SBA-15 as highly selective catalysts in the oxidative dehydrogenation of propane. *J. Catal.* **2004**, *224*, 417–428.
- (22) Zhao, C.; Wachs, I. E. An operando Raman, IR, and TPRS spectroscopic investigation of the selective oxidation of propylene to acrolein over a model supported vanadium oxide monolayer catalyst. *J. Phys. Chem. C* **2008**, *112*, 11363–11372.
- (23) Fukudome, K.; Ikenaga, N.-o.; Miyake, T.; Suzuki, T. Oxidative dehydrogenation of alkanes over vanadium oxide prepared with V(*t*-BuO)<sub>3</sub>O and Si(OEt)<sub>4</sub> in the presence of polyethyleneglycol. *Catal. Today* **2013**, *203*, 10–16.
- (24) Konya, T.; Katou, T.; Murayama, T.; Ishikawa, S.; Sadakane, M.; Buttrey, D.; Ueda, W. An orthorhombic Mo<sub>3</sub>VO<sub>x</sub> catalyst most active for oxidative dehydrogenation of ethane among related complex metal oxides. *Catal. Sci. Technol.* **2013**, *3*, 380–387.
- (25) Oyama, S. T. Adsorbate bonding and the selection of partial and total oxidation pathways. *J. Catal.* **1991**, *128*, 210–217.
- (26) Adamski, A.; Sojka, Z.; Dyrek, K.; Che, M.; Wendt, G.; Albrecht, S. Surface heterogeneity of zirconia-supported V<sub>2</sub>O<sub>5</sub> catalysts. The link between structure and catalytic properties in oxidative dehydrogenation of propane. *Langmuir* **1999**, *15*, 5733–5741.
- (27) Shin, M. Y.; Chung, K. S.; Hwang, D. W.; Chung, J. S.; Kim, Y. G.; Lee, J. S. Behavior of lattice oxygen in mixtures of V<sub>2</sub>O<sub>5</sub> and Bi<sub>2</sub>O<sub>3</sub>. *Langmuir* **1999**, *16*, 1109–1113.
- (28) Ballarín, N.; Cavani, F.; Cericola, A.; Cortelli, C.; Ferrari, M.; Trifiro, F.; Capannelli, G.; Comite, A.; Catani, R.; Cornaro, U. Supported vanadium oxide-based catalysts for the oxidative dehydrogenation of propane under cyclic conditions. *Catal. Today* **2004**, *91–92*, 99–104.
- (29) Venkov, T. V.; Hess, C.; Jentoft, F. C. Redox properties of vanadium ions in SBA-15-supported vanadium oxide: An FTIR spectroscopic study. *Langmuir* **2006**, *23*, 1768–1777.
- (30) Rossetti, I.; Mancini, G. F.; Ghigna, P.; Scavini, M.; Piumetti, M.; Bonelli, B.; Cavani, F.; Comite, A. Spectroscopic enlightening of the local structure of VO<sub>x</sub> active sites in catalysts for the ODH of Propane. *J. Phys. Chem. C* **2012**, *116*, 22386–22398.
- (31) Chen, M. S.; Wang, X. V.; Zhang, L. H.; Tang, Z. Y.; Wan, H. L. Active surfaces for CO oxidation on palladium in the hyperactive state. *Langmuir* **2010**, *26*, 18113–18118.
- (32) Campbell, R. A.; Goodman, D. W. A new design for a multitechnique ultrahigh vacuum surface analysis chamber with high pressure capabilities. *Rev. Sci. Instrum.* **1992**, *63*, 172–174.
- (33) Chen, M. S.; Kumar, D.; Yi, C. W.; Goodman, D. W. The promotional effect of gold in catalysis by palladium–gold. *Science* **2005**, *310*, 291–293.
- (34) Poelman, H.; Vennik, J.; Dalmai, G. A HREELS study of the V<sub>2</sub>O<sub>5</sub> (001) surface phonon spectrum. *J. Electron Spectrosc. Relat. Phenom.* **1987**, *44*, 251–262.
- (35) Wong, G. S.; Concepcion, M. R.; Vohs, J. M. Reactivity of monolayer V<sub>2</sub>O<sub>5</sub> films on TiO<sub>2</sub>(110) produced via the oxidation of vapor-deposited vanadium. *Surf. Sci.* **2003**, *526*, 211–218.
- (36) Dupuis, A. C.; Abu Hajja, M.; Richter, B.; Kühlenbeck, H.; Freund, H. J. V<sub>2</sub>O<sub>5</sub>(0001) on Au(111) and W(110): Growth, termination and electronic structure. *Surf. Sci.* **2003**, *539*, 99–112.
- (37) Schoiswohl, J.; Sock, M.; Eck, S.; Surnev, S.; Ramsey, M. G.; Netzer, F. P.; Kresse, G. Atomic-level growth study of vanadium oxide nanostructures on Rh(111). *Phys. Rev. B* **2004**, *69*, 155403.
- (38) Surnev, S.; Kresse, G.; Sock, M.; Ramsey, M. G.; Netzer, F. P. Surface structures of ultrathin vanadium oxide films on Pd(111). *Surf. Sci.* **2001**, *495*, 91–106.
- (39) The statistic lengths of the perimeters of the V<sub>2</sub>O<sub>5</sub> 2D domains as a function of the V<sub>2</sub>O<sub>5</sub> coverage ( $\theta$ ) displayed in Figure 3B were computed by assuming that the coverage increase first results in the increase of the number of the well-separate 2D domains with a same size (gray squares in Figure 3B) until that a half of the surface area is covered by the 2D domains ( $\theta = 0.5$ ); further increasing the coverage then leads to locate a square domain (white) in between the gray square domains which eliminates a square boundary of 4l. Such an ideal case achieves a maximum length at  $\theta = 0.5$  (Figure 3B, curve a). In real cases, the size of 2D domains will also increase as the coverage increases, resulting in that the maximum lengths occur at  $\theta < 0.5$  ML. Enlarge factors of 0.5%, 1%,

and 10%, respectively, are used for Figure 3B, curves b–d, respectively. Beside the increase of the domain sizes as the coverage increases, some domains may merge together resulting in a slow increase of domain boundary length (a probability of 1% was assumed for Figure 3B, curve e).

(40) Cheng, M.-J.; Chenoweth, K.; Oxgaard, J.; van Duin, A.; Goddard, W. A. Single-site vanadyl activation, functionalization, and reoxidation reaction mechanism for propane oxidative dehydrogenation on the cubic  $V_4O_{10}$  cluster. *J. Phys. Chem. C* **2007**, *111*, 5115–5127.

(41) Berlowitz, P. J.; Peden, C. H. F.; Goodman, D. W. Kinetics of carbon monoxide oxidation on single-crystal palladium, platinum, and iridium. *J. Phys. Chem.* **1988**, *92*, 5213–5221.

(42) Campbell, C. T.; Ertl, G.; Kuipers, H.; Segner, J. A molecular beam study of the adsorption and desorption of oxygen from a Pt(111) surface. *Surf. Sci.* **1981**, *107*, 220–236.

(43) Guo, X. C.; Hoffman, A.; Yates, J. J. T. Adsorption kinetics and isotopic equilibration of oxygen adsorbed on the Pd(111) surface. *J. Chem. Phys.* **1989**, *90*, 5787–5792.

(44) Chen, K. D.; Bell, A. T.; Iglesia, E. The relationship between the electronic and redox properties of dispersed metal oxides and their turnover rates in oxidative dehydrogenation reactions. *J. Catal.* **2002**, *209*, 35–42.

(45) Chang, H.; Phillips, J.; Heck, R. Catalytic synergism in physical mixtures. *Langmuir* **1996**, *12*, 2756–2761.

(46) Kao, C. L.; Madix, R. J. The adsorption dynamics of molecular methane, propane, and neopentane on Pd(111): Theory and experiment. *J. Phys. Chem. B* **2002**, *106*, 8248–8257.

(47) Nykänen, L.; Honkala, K. Density functional theory study on propane and propene adsorption on Pt(111) and PtSn alloy surfaces. *J. Phys. Chem. C* **2011**, *115*, 9578–9586.

(48) Yao, Y. F. Y. Oxidation of alkanes over noble metal catalysts. *Ind. Eng. Chem. Prod. Res. Dev.* **1980**, *19*, 293–298.

(49) Weaver, J. F.; Hakanoglu, C.; Hawkins, J. M.; Asthagiri, A. Molecular adsorption of small alkanes on a PdO(101) thin film: Evidence of sigma-complex formation. *J. Chem. Phys.* **2010**, *132*, 024709.

(50) Chiba, A.; Komoda, M.; Kosumi, T.; Nanba, T.; Azuma, N.; Ueno, A. Difference in catalytic combustion of propane and propene on Pt/ $Al_2O_3$  catalyst. *Chem. Lett.* **1999**, 801–802.

(51) Arata, K.; Matsushashi, H.; Hino, M.; Nakamura, H. Synthesis of solid superacids and their activities for reactions of alkanes. *Catal. Today* **2003**, *81*, 17–30.

(52) Hwang, C. C.; Chen, X. R.; Wong, S. T.; Chen, C. L.; Mou, C. Y. Enhanced catalytic activity for butane isomerization with alumina-promoted tungstated mesoporous zirconia. *Appl. Catal., A* **2007**, *323*, 9–17.

(53) Taylor, M. N.; Carley, A. F.; Davies, T. E.; Taylor, S. H. The oxidative dehydrogenation of propane using vanadium oxide supported on nanocrystalline ceria. *Top. Catal.* **2009**, *52*, 1660–1668.

(54) Vajda, S.; Pellin, M. J.; Greeley, J. P.; Marshall, C. L.; Curtiss, L. A.; Ballentine, G. A.; Elam, J. W.; Catillon-Mucherie, S.; Redfern, P. C.; Mehmood, F.; Zapol, P. Subnanometre platinum clusters as highly active and selective catalysts for the oxidative dehydrogenation of propane. *Nat. Mater.* **2009**, *8*, 213–216.

(55) Silberova, B.; Fathi, M.; Holmen, A. Oxidative dehydrogenation of ethane and propane at short contact time. *Appl. Catal., A* **2004**, *276*, 17–28.

(56) Dadyburjor, D. B.; Das, T. K.; Kugler, E. L. Reactions for the partial oxidation of propane over Pt-on-Ceria. *Appl. Catal., A* **2011**, *392*, 127–135.

(57) Centi, G.; Perathoner, S. Reaction mechanism and control of selectivity in catalysis by oxides: Some challenges and open questions. *Int. J. Mol. Sci.* **2001**, *2*, 183–196.

(58) Heynderickx, P. M.; Thybaut, J. W.; Poelman, H.; Poelman, D.; Marin, G. B. Kinetic modeling of the total oxidation of propane over anatase and vanadia sputter deposited catalysts. *Appl. Catal., B* **2009**, *90*, 295–306.

(59) Garcia, T.; Solsona, B.; Murphy, D. M.; Antcliff, K. L.; Taylor, S. H. Deep oxidation of light alkanes over titania-supported palladium/vanadium catalysts. *J. Catal.* **2005**, *229*, 1–11.

(60) Baldychev, I.; Gorte, R. J.; Vohs, J. M. The impact of redox properties on the reactivity of  $V_2O_5/Al_2O_3$  catalysts. *J. Catal.* **2010**, *269*, 397–403.